A Joint Inversion of Ground Deformation and Focal Mechanisms Data for Magmatic Source Modelling

Flavio Cannavò, Danila Scandura, Mimmo Palano & Carla Musumeci

Pure and Applied Geophysics
pageoph

ISSN 0033-4553

Pure Appl. Geophys.
DOI 10.1007/s00024-013-0771-x

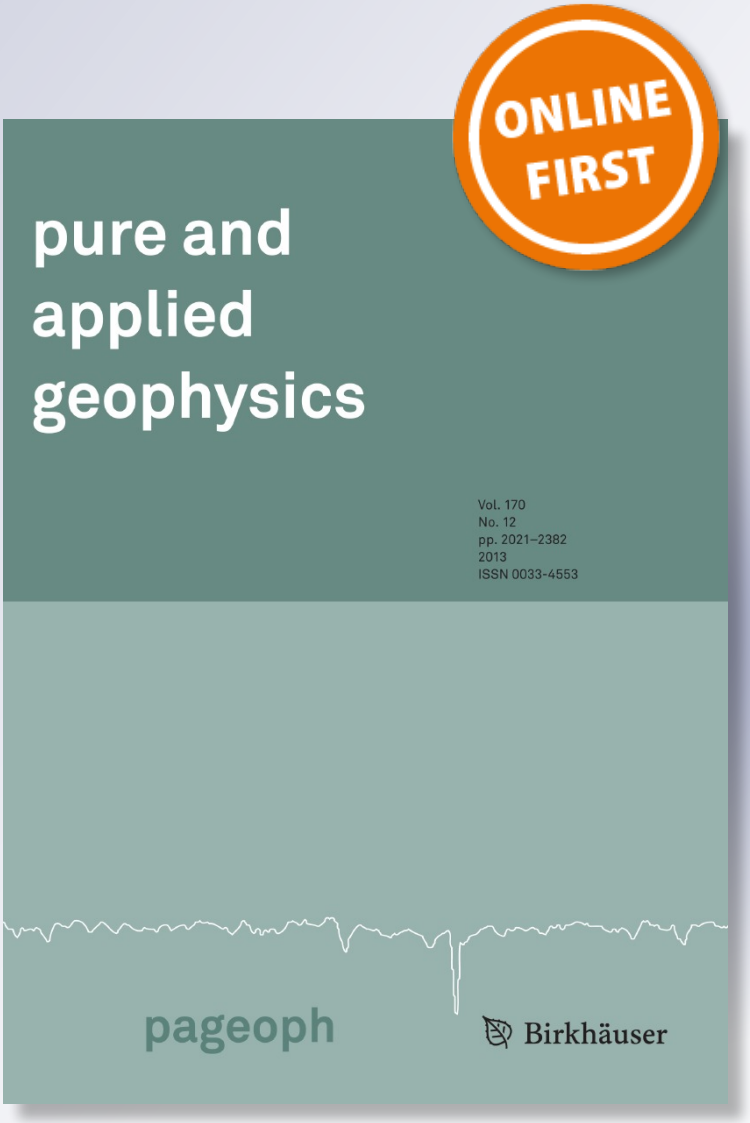

Springer

Pure Appl. Geophys.

DOI 10.1007/s00024-013-0771-x

Pure and Applied Geophysics

A Joint Inversion of Ground Deformation and Focal Mechanisms Data for Magmatic Source Modelling

Flavio Cannavò,[1] Danila Scandura,[1] Mimmo Palano,[1] and Carla Musumeci[1]

Abstract—The paucity of geodetic data acquired on active volcanoes can make the understanding of modelling magmatic systems quite difficult. In this study, we propose a novel approach, which allows improving the parameter estimation of analytical models of magmatic sources (e.g., shape, depth, dimensions, volume change, etc.) by means of a joint inversion of surface ground deformation data and *P*-axes of focal plane solutions. The methodology is first verified against a synthetic dataset of surface deformation and strain within the medium, and then applied to real data from an unrest episode occurred before the May 13 2008 eruption at Mt. Etna (Italy). The main results clearly indicate the joint inversion improves the accuracy of the estimated source parameters by about 70 %. The statistical tests indicate that the source depth is the parameter with the highest increment of accuracy. In addition, a sensitivity analysis confirms that displacements data are more useful to constrain the pressure and the horizontal location of the source than its depth, while the *P*-axes better constrain the depth estimation.

Key words: GPS, Mt. Etna volcano, pressure source, modelling.

1. Introduction

Seismicity and ground deformation represent the principal geophysical methods for volcano monitoring and provide important constraints on subsurface magma movements. The occurrence of migrating seismic swarms, as observed at several volcanoes worldwide, are commonly associated with dike intrusions (see Brandsdottir and Einarsson 1979; Rubin *et al.* 1998; Patanè *et al.* 2003; Barberi *et al.* 2004; Segall 2013). In addition, on active volcanoes, (de)pressurization and/or intrusion of magmatic bodies stress and deform the surrounding crustal rocks, often causing earthquakes randomly distributed in time within a volume extending about 5–10 km from the wall of the magmatic bodies (Umakoshi *et al.* 2001; Roman 2005; Fig. 1).

Several mathematical models have been developed to quantify both the magmatic body parameters (e.g., shape, depth, dimensions, internal volume change, etc.) (see Segall 2010 for an overview) and the expected ground deformation pattern at the Earth's surface. Therefore, by comparing the observed surface deformation to that computed by mathematical models, quantitative estimations of source location, geometry, and volume change can be inferred. However, modelling of surface deformation generally belongs to the so called ill-posed inverse problem (Atefi Monfared and Rothenburg 2011), which can show a weak stability of the estimated parameters (Tikhonov and Arsenin 1977) also depending on the spatial data distribution. Indeed, in regions where the spatial coverage of geodetic observations is inadequate, any inversion for modelling of surface deformation is bound to be poorly constrained by the limited data. Model assumptions, simplifications and data uncertainty further complicate the interpretation. Improvements of the model could be achieved by increasing the spatial coverage of the monitoring network; however, this is often not possible.

Despite advances in space-based, geodetic and seismic networks having significantly improved volcano monitoring in the last decades on an increasing worldwide number of volcanoes, quantitative models relating deformation and seismicity are not common. Based on the seismicity-rate theory of Dieterich (1994), recently Segall (2013) has evidence that deformation and seismicity can be integrated into self-consistent inversions for the spatio-temporal

[1] Istituto Nazionale di Geofisica e Vulcanologia, Osservatorio Etneo, Sezione di Catania, P.zza Roma, 2, 95123 Catania, Italy. E-mail: flavio.cannavo@ct.ingv.it; danila.scandura@ct.ingv.it; mimmo.palano@ct.ingv.it; carla.musumeci@ct.ingv.it

Published online: 21 January 2014

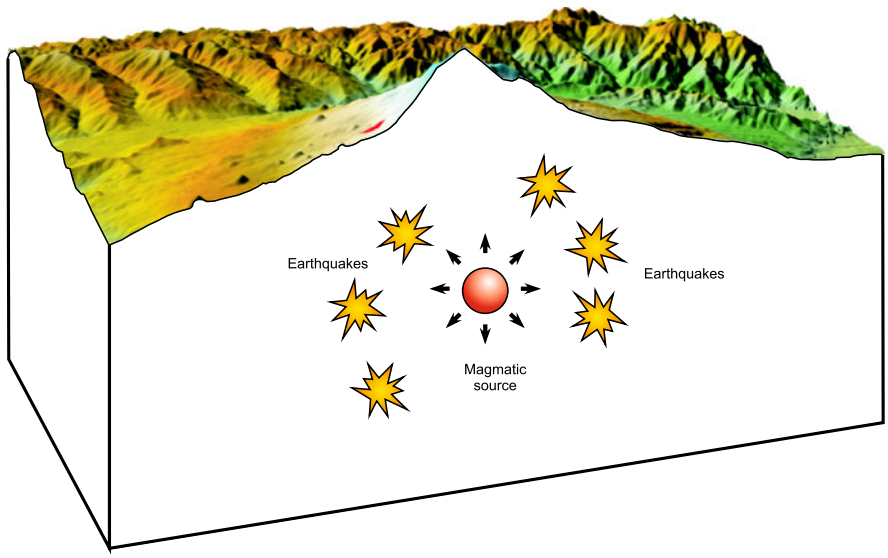

Figure 1
Cartoon illustrating the relationship between the pressurization of a magmatic body and the occurrence of seismicity in the surrounding crustal rock

evolution of dike geometry and excess magma pressure. Although this approach is currently limited to a linkage between deformation and seismicity due to a propagating magmatic intrusion, it could lead to an improved resolution over existing methods and, perhaps, to improved real-time forecasts (see SEGALL 2013 and references therein for an overview).

The observation of several episodes of volcanic unrest throughout the world, where the movement of magma through the shallow crust was able to produce local rotation of the ambient stress field (NAKAMURA *et al.* 1977; MUSUMECI *et al.* 2000; ROMAN *et al.* 2004; BONANNO *et al.* 2011), introduces an opportunity to improve the estimate of the parameters of a deformation source. In particular, during these episodes of volcanic unrest, a radial pattern of *P*-axes of the focal mechanism solutions, similar to that of ground deformation, has been observed. Therefore, taking into account additional information from focal mechanisms data, we propose a novel approach to volcanic source modelling based on the joint inversion of deformation and focal plane solutions assuming that both observations are due to the same source. In the following sections, after a full description of the method and its verification, we present a test on a real case study from Mt. Etna (Italy).

2. Method Overview

In volcanic areas, the observed deformation is usually modelled by means of analytical solutions (e.g., BATTAGLIA and HILL 2009) which provide the expected deformation field at the free surface of an elastic medium. Because earthquakes, instead, occur within the medium, we looked at those analytical models able to describe the strain also within the medium. In the seismological literature, *P* (for pressure) and *T* (for tension) are the principal axes of the moment tensor, with *P* being the axis of maximum compression and *T* the axis of minimum compression (Fig. 2). Taking into account the orientation of the principal strain axis, the expected deformation strain tensor related to the pressure sources can be computed at the earthquake hypocenter. In order to calculate the strain tensor, we adopted the infinitesimal strain theory applied to elastic materials, which assumes that the displacements and their gradients are small if compared to the unit. In that case, the linearized Lagrangian and Eulerian strain tensors (i.e., neglecting the non-linear or second-order terms of the finite strain tensor) are almost the same and can be approximated by the infinitesimal strain tensor known as Cauchy's strain tensor:

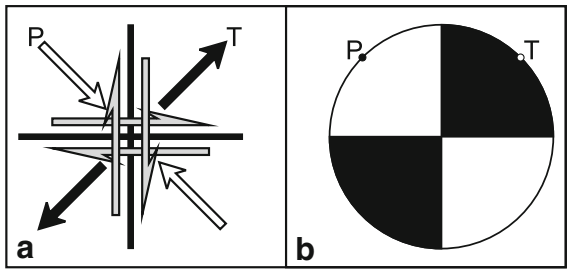

Figure 2
Schematic representation of an activated fault and the direction of slip on it from an earthquake as **a** double couple force system and equivalent force dipoles (*P*- and *T*-axes), **b** stereographic projection (known also as focal mechanism and/or "beachball" solution) with two intersecting planes (nodal planes). *P*- and the *T*-axes represent the axes of maximum shortening and maximum lengthening respectively, bisecting the quadrants

$$\varepsilon_{ij} = \frac{1}{2}\left(\frac{\partial u_i}{\partial x_j} + \frac{\partial u_j}{\partial x_i}\right), \tag{1}$$

where u is the vector of infinitesimal deformation of a continuum body in a coordinate system (x_i, x_j, x_k). Since the strain tensor is real and symmetric, it can be rotated into a principal system [n_1, n_2, n_3] where all off-diagonal elements are zero:

$$\bar{\varepsilon} = \begin{bmatrix} \varepsilon_1 & 0 & 0 \\ 0 & \varepsilon_2 & 0 \\ 0 & 0 & \varepsilon_3 \end{bmatrix}. \tag{2}$$

The components of the strain tensor in the [n_1, n_2, n_3] coordinate system represent the principal strains and the directions n_i refer to the directions of the principal strain. Since there are no shear strain components in this coordinate system, the principal strains represent the maximum and minimum stretches of an elemental volume.

The principal strains can be found by using an eigenvalue decomposition by solving the linear system:

$$(\bar{\varepsilon} - \varepsilon_i I)n_i = \bar{0} \tag{3}$$

where I is the identity matrix.

This system of equations is equivalent to finding the vector n_i along which the strain tensor becomes a pure stretch with no shear component. Hence, by analyzing the principal strain directions at some earthquake hypocenter, we can fit the *P*-axes of focal mechanism and the direction of maximum compression due to a volcanic source. We aim to find a source able to fit at the same time the strain data coming from earthquakes and the deformation data coming from GPS stations.

3. Joint Inversion of Strain and Deformation Data

The proposed joint inversion of strain (i.e., the compression along the *P*-axes) and ground deformation data, is implemented by finding the source that minimizes the misfit between: (1) the measured and modeled displacements; (2) the angles between the *P*-axes and the modeled direction of maximum compression. Before applying the methodology to a real case, we carried out some preliminary tests in order to assess the quality of results and to quantify the improvements of the proposed joint inversion with respect to the classical inversion based only on ground deformation data. The statistical tests have been performed taking into account the results coming from 100 trials.

For each trial, we generated a synthetic dataset of surface deformation and strain within the medium (i.e., *P*-axes) by adopting the analytical solutions developed for an homogenous and isotropic half-space by McTigue (1987) in the general formulation describing also the internal deformation (see Battaglia *et al.* 2013 for an overview). To overcome the unfeasibility of this formulation for *P*-axes calculated below the source, and recalling the isotropy assumption of the infinity half-space, we considered the direction of maximum strain as radial from the source. Then we performed two different inversions: in a first one we inverted just for the surface deformation, while in a second one we jointly inverted for both the surface deformation and the *P*-axes. In particular, we considered three-dimensional displacements calculated at four points [hereinafter point of measurement (PoM)] on the surface and four *P*-axes calculated within the medium. In order to avoid biases due to network topology, the stations were randomly chosen by sampling a normal distribution with standard deviation (SD) of 7 km. For the same reason the four *P*-axes locations were normally distributed with a SD of 7 km in the horizontal components and 3 km in the vertical component. In each trial we added 20 levels of noise to the synthetic

dataset. The noise had a Gaussian distribution characterized by a zero mean and SDs linearly proportional to 3 mm for displacements and 0.5° for *P*-axes angles. The assumption of a point source of dilatation as the McTigue source (i.e., depth much greater than size) implies that the magma-chamber radius (r) and pressure change (ΔP) are inseparable being $\Delta P r^3$ the strength of the point singularity (Battaglia *et al.* 2013). We fixed the radius to 400 m, as a realistic value, to avoid this ambiguity. We calculated the absolute error of each model parameter which was estimated after an inversion of the noisy synthetic data. The algorithm used for the non-linear inversions was the Levenberg–Marquardt algorithm (LMA) (Pujol 2007). When only displacement data were considered, the optimization goal was to minimize the normalized Chi squared of the model residues expressed as:

$$\chi_d^2 = \frac{1}{N_d} \sum_i \left(\frac{m_i - d_i}{\sigma_{d_i}} \right)^2, \quad (4)$$

where N_d is the total number of displacement components, m_i is the modeled ith displacement component, d_i is the ith displacement component and σ_{d_i} is its associated error. In the joint inversion of displacement and *P*-axes data, the fitness function was the sum of the normalized Chi squared of both the two kind of residues expressed as:

$$\chi_J^2 = \frac{1}{N_d} \sum_i \left(\frac{m_i - d_i}{\sigma_{d_i}} \right)^2 + \frac{1}{N_P} \sum_i \left(\frac{\varphi(a_i, P_i)}{\sigma_{P_i}} \right)^2, \quad (5)$$

where N_P is the total number of *P*-axes, φ is the angular distance between the modeled ith *P*-axis a_i and the synthetic one P_i, while σ_{P_i} is its associated error.

Finally, we compared the estimated source parameters obtained from the two inversions. For this purpose, we calculated the increment of precision for each parameter of the model in terms of percentage of reduction of the absolute error for the parameters when the joint inversion is adopted. In Fig. 3a the increment of precision of depth, horizontal position and pressure changes is shown. The percentage refers to the mean increment of precision of model parameters for all the 100 simulations. In order to estimate the dispersion of the increment of precision, we associated a SD to these mean values. The comparison clearly indicates that the introduction of *P*-axes data always improves the quality of source estimation from noisy data. We can consider a threshold on the noise level on data that leads to improvements on source parameter estimation above a chosen percentage. In addition, note that the almost flat interval (Fig. 3a) with the highest improvements ends with a noise level on data of about 9 cm at 3-Sigma for the displacement components and 15 degrees for the *P*-axes angles. Moreover, it is worth noting that the source depth is the parameter with the highest increment of accuracy (in average 79 % against the 59 and 63 % of horizontal position and pressure, respectively). Notice that the curve related to the source depth (Fig. 3a) is the less scattered among the considered parameters, and it is also the less sensitive to the noise level of the input data. Thus, *P*-axes allow for improving the constrain on the depth estimation of the magma source. This is confirmed also by the sensitivity analysis we performed. Indeed, we calculated the global sensitivity (S) coefficients (Cannavó 2012) to study the variance propagation in the inverse problem, from data to model parameters. We carried out Monte Carlo simulations on an inverse problem based on two displacement stations and two *P*-axes, in order to estimate the sensitivity coefficients for the source parameters. Results, shown in Table 1, point out that the global sensitivity of the source depth to *P*-axes angles is much greater than to displacement data. Thus, the source depth is more constrained to *P*-axes than to three-dimensional displacements at the surface. The horizontal location of the source is strongly sensitive to displacement data ($S \approx 0.87$), and being $S \approx 0.60$ for *P*-axis angles, we can assert that displacements constrain the horizontal position better than the *P*-axes. Looking at Table 1, the results suggest that displacements data are more useful to constrain the pressure and the horizontal location of the source than its depth. Furthermore, *P*-axes most affect the depth parameter than the horizontal location while the source pressure is independent from them being 0 for its sensitivity, as expected.

In addition to the simulations described above, where we just added the *P*-axes data to the surface deformation, we also considered the simulations

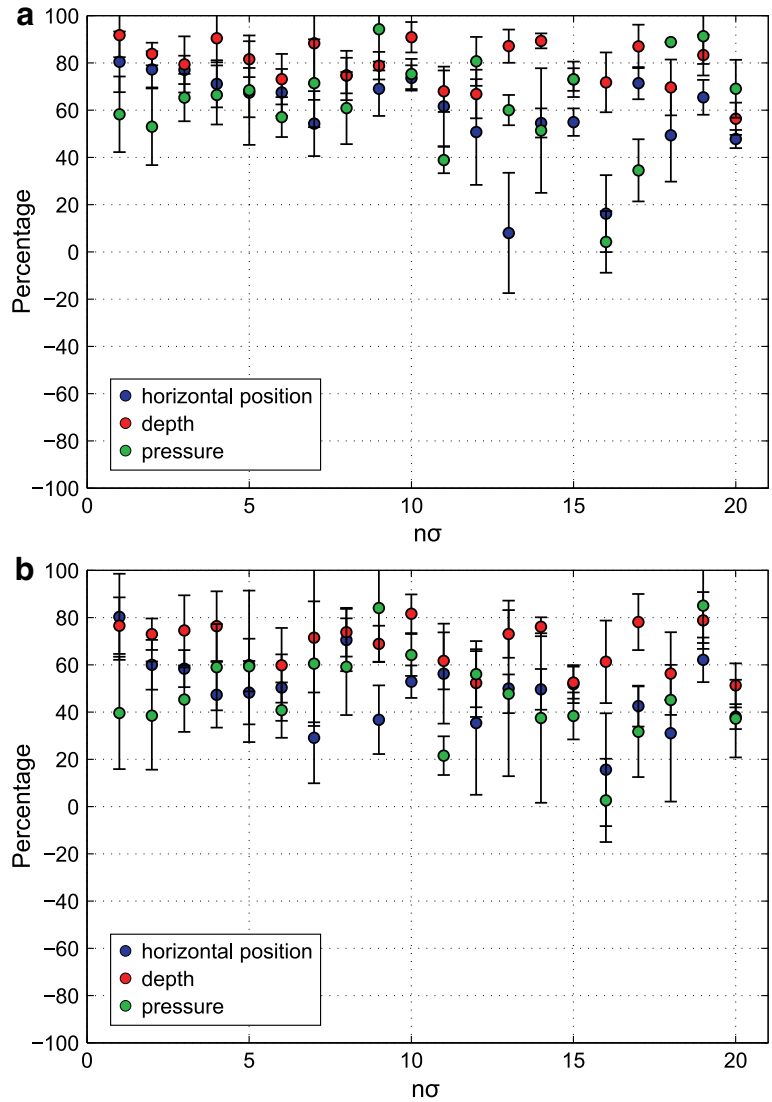

Figure 3
Increment of precision for each parameter of the model in terms of percentage of reduction of the absolute error for the three parameters when the joint inversion is adopted instead of the traditional one based only on displacement data. The percentage refers to the mean increment of precision of model parameters for all the 100 simulations. **a** Results for four PoMs and four *P*-axes against only four PoMs; **b** results for three PoMs displacements and three *P*-axes against only five PoMs

where part of the surface deformation (used as input for the traditional inversion) is substituted with *P*-axes data (used as input for the joint inversion). In this second case, in fact, in order to maintain the same number of measurables, and observing that each PoM consists of three displacement components while each *P*-axis consisting of two angles (azimuth and dip), we chose to invert a set of five PoMs for the classical inversion and only three of them for the joint inversion with three *P*-axes. In this way we obtained results independent from the number of system equations. Also in this second case, we performed some statistical tests taking into account the results coming from 100 trials. In particular, Fig. 3b shows the percentage of error reduction in source estimation with the joint inversion of three PoMs and three

Table 1

Coefficients of global sensitivity of source parameters for both displacements and P-axes in a Monte Carlo simulation

Parameters	Three-dimensional displacements	*P*-axes
Source depth	0.56 ± 0.05	0.82 ± 0.07
Source pressure	0.99 ± 0.01	0.00 ± 0.01
Source horizontal position	0.87 ± 0.05	0.60 ± 0.08

P-axes instead of the classical inversion of five PoMs, thus, maintaining constant the number of constrains for both the inversions. The visual comparison between Fig. 3a, b shows that the quality of model estimation is, on average, higher if we add the seismic data instead of replacing them to part of the displacement data. In the latter case the quality of the estimated model parameters (although always positive, hence, outperforming the classical inversion) is more scattered with the noise level of data compared to the former case. Nevertheless, the general considerations set out above for the results in Fig. 3a can be made for the Fig. 3b, revealing a good reliability for the proposed approach.

4. A Real Case Study

We tested the proposed approach by studying an unrest episode that occurred at Mt. Etna during the January 1–May 12 2008 time interval. This episode represents an inflation event occurring before the beginning of the May 13 2008 Mt. Etna eruption (Aloisi *et al.* 2011; Bruno *et al.* 2012) that was recorded both by surface deformation and seismological observations.

We processed the GPS data using GAMIT/GLOBK (Herring *et al.* 2010) following the strategy described in Palano *et al.* (2011). We referred the estimated GPS velocities to the Etn@ref reference frame (Palano *et al.* 2010) enabling us to isolate the Mt. Etna volcanic deformation from the background tectonic deformation. *P*-axes available for the same time interval (Alparone *et al.* 2012) were used for the inversions. Focal plane solutions from *P*-wave first motions were determined by considering the fault plane fit grid-search algorithm of Reasenberg and Oppenheimer (1985). The dataset consisted of 21 well-constrained FPSs (Table 2) with average location

Table 2

Date, origin time (OT), magnitude, number of polarities (Np) hypocentral and focal parameters of earthquakes used for the joint inversion

Id	Date	OT	Lat. N	Long. E	Depth (km)	*M*	Np	Nodal plane			*P*-axis	
								Strike	Dip	Rake	Azm	Plng
01	07/01/2008	17.45	37.682	14.948	11.59	2.7	18	280	75	0	236	11
02	07/01/2008	18.13	37.684	14.953	11.68	2.6	14	0	90	160	47	14
03	07/01/2008	18.30	37.674	14.956	12.63	2.4	10	60	55	−20	26	37
04	07/01/2008	18.32	37.681	14.956	13.13	2.2	19	75	60	10	31	14
05	07/01/2008	18.36	37.681	14.953	11.41	2.3	28	50	60	−10	12	27
06	12/01/2008	1.51	37.742	14.891	19.19	3.2	28	330	70	10	285	7
07	30/01/2008	4.23	37.772	15.132	10.27	2.3	20	110	55	10	67	18
08	02/02/2008	2.53	37.667	15.100	5.44	2.1	22	55	90	120	118	38
09	08/02/2008	2.16	37.736	15.120	6.04	2.4	25	120	80	−10	76	14
10	14/02/2008	22.58	37.810	15.089	0.73	2.7	12	290	90	40	57	27
11	14/02/2008	23.52	37.807	15.091	1.38	2.8	16	285	90	10	60	7
12	11/03/2008	15.23	37.826	15.071	11.32	2.1	9	75	80	120	141	29
13	11/03/2008	16.29	37.831	15.070	11.49	2.2	11	105	75	60	218	24
14	24/03/2008	2.45	37.742	15.089	6.44	2.1	14	115	65	−30	76	38
15	05/04/2008	2.40	37.769	15.088	6.74	2.4	22	100	65	−10	60	24
16	09/04/2008	4.14	37.732	15.132	8.65	3.5	32	110	55	−10	74	30
17	20/04/2008	7.47	37.632	15.022	0.72	3.2	26	65	50	70	169	3
18	01/05/2008	21.05	37.806	15.038	0.16	3.5	19	270	90	10	45	7
19	01/05/2008	22.16	37.806	15.033	0.22	2.1	9	325	45	80	242	0
20	02/05/2008	12.04	37.819	15.075	−1.96	3	10	295	80	10	249	0
21	02/05/2008	16.14	37.805	15.042	0.2	2.6	8	40	60	−140	255	48

Depths are referred to sea level

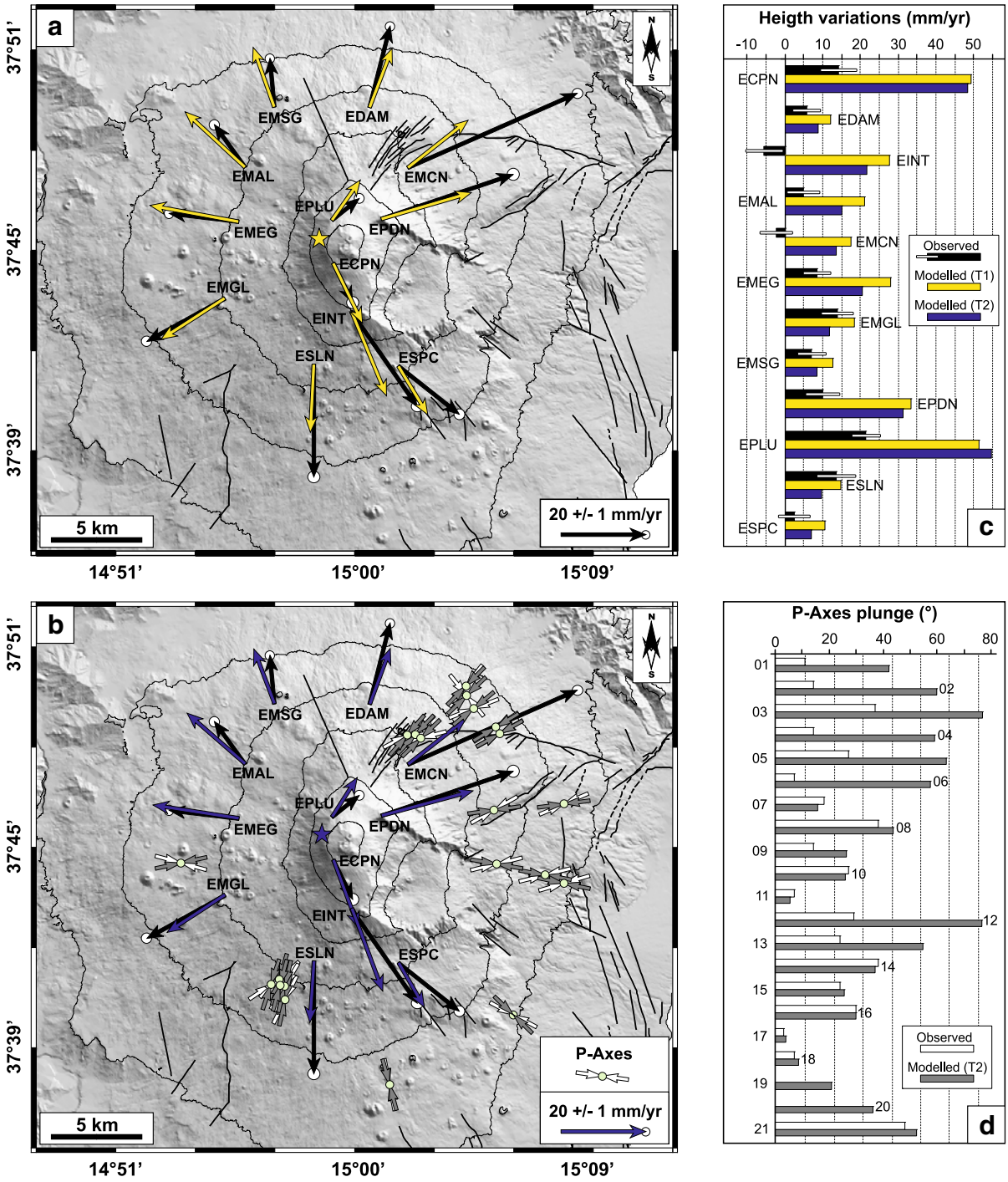

Figure 4

a Observed (*black arrows*) and modelled (*yellow arrows*) horizontal velocity field for *T*1 test; **b** observed (*black arrows*) and modelled (*blue arrows*) horizontal velocity field for *T*2 test; the horizontal projections of observed and modelled *P*-axes are reported as *white* and *gray arrows*, respectively. For each test, the modelled source (*star*) is also reported. **c** Observed and modelled vertical velocities for *T*1 and *T*2 tests. **d** Observed and modelled *P*-axes plunge for *T*2 test. See Tables 1 and 3 for details

uncertainties of 0.23 (±0.10 km SD) and 0.25 (±0.10 km SD) in the horizontal and vertical directions, respectively, and averaged uncertainties in fault orientation parameters, strike, dip and rake, smaller than 20° (Alparone *et al.* 2012).

The inversions were performed by using the LMA approach and assuming the McTigue (1987) formalism. In addition, the same starting point and the same parameter space have been used. As elevation of the half-space surface we adopted the average elevation of GPS stations used for the inversions (ca. 2,060 m a.s.l.), while 30 GPa and 0.25 were assumed as values for μ and Poisson's ratio, respectively. The rigidity chosen corresponds to a typical value of crustal rigidity commonly used in modelling works (e.g., Williams and Wadge 2000; Trasatti *et al.* 2003; Palano *et al.* 2008) which is found to be an average rigidity value for Mt. Etna crust (Chiarabba *et al.* 2000). Estimation of the uncertainties in best-fitting parameters was performed by adopting a Jackknife sampling method (Efron 1982). During each inversion the radius of the source was fixed to the value of 400 m.

As a first test, we performed an inversion (labelled *T*1) by using only the GPS surface velocity deformation field as input. The best result depicts a source centred at 5.9 km depth beneath the upper western flank of the volcano edifice (Fig. 4a; Table 3). As a second test, we performed a new inversion (labelled *T*2) by taking into account also the *P*-axes of FPSs available for the investigated time period. The best result depicts a source located ~0.35 km SW and ~1.2 km shallower with respect to the source obtained in *T*1 (Fig. 4a; Table 3).

Taking into account the uncertainties of the source parameters we can assert that the horizontal position of the source and its pressure change remain the same for both the inversions, while for the source depth, the inversions show non-overlapping solutions. According to the results here obtained from the synthetic test, we are more confident with the outcome from the joint inversion.

Table 3

Parameters of the modelled sources inferred for each test

Parameters	*T*1	*T*2
Easting (m)	497,928 ± 191	498,231 ± 202
Northing (m)	4,178,783 ± 148	4,178,952 ± 215
Depth (m)	5,889 ± 416	4,723 ± 227
Radius (m)	400 (fixed value)	400 (fixed value)
ΔP (Pa)	$313 \pm 35 \times 10^6$	$294 \pm 33 \times 10^6$

Depth refers to the elevation of the half-space surface, assumed as the average elevation of GPS stations used for inversions (ca. 2,060 m). For each model parameter, errors (at 95 % of confidence) were estimated by adopting a Jackknife-sampling method (Efron 1982)

5. *Concluding Remarks*

In this study, we set out a novel approach allowing for improvement in the estimate of the parameters (e.g., shape, depth, dimensions, internal magma changes, etc.) of magmatic sources by a joint inversion of both the velocity/displacement field (observed at the surface of the volcano edifice) and the FPSs *P*-axis (computed for earthquakes occurring within the volcanic edifice).

By performing some statistical tests on the results coming from 100 trials based on a synthetic dataset, we observed that the joint inversion improves the quality of the estimated source parameters of about 70 % in terms of precision. These tests clearly indicate that, among the parameters, the source depth is the one with the highest increment of accuracy. Moreover, a sensitivity analysis confirms that displacements data are more useful to constrain the pressure and the horizontal location of the source than its depth, while *P*-axes better constrain the depth estimation.

The methodology was applied to the real data coming from an unrest episode occurred before the May 13 2008 eruption at Mt. Etna. The joint inversion infers a source shallower than the one obtained from the classical inversion. By considering the results coming from the synthetic tests, we retain this solution more reliably.

In conclusion, our approach can help in improving the estimate of the parameters of the deformation source for those areas where the spatial coverage of geodetic observations is poor. In addition, it could be successfully adopted for other kinds of deformation sources as long as they are defined also within the medium.

Acknowledgments

We thank two anonymous reviewers for their critical reviews and constructive comments that greatly improved the paper. We greatly appreciated the suggestions by the Editor Eugenio Carminati. We also thank S. Conway for correcting and improving the English language of this manuscript.

References

Aloisi, M., Mattia, M., Ferlito, C., Palano, M., Bruno, V. and Cannavò, F. (2011). *Imaging the multilevel magma reservoir at Mt. Etna volcano (Italy)*, Geophys. Res. Lett., *38*, L16306, doi:10.1029/2011GL048488.

Alparone, S., Barberi, G., Cocina, O., Giampiccolo, E., Musumeci, C. and Patanè, D. (2012). *Intrusive mechanism of the 2008–2009 Mt. Etna eruption: Constraints by tomographic images and stress tensor analysis*, J. Volc. Geotherm. Res., *229–230*, 50–63, doi:10.1016/j.jvolgeores.2012.04.001.

Atefi Monfared, K., and Rothenburg, L. (2011). *Ground surface displacements and tilt monitoring for reconstruction of reservoir deformations*, International Journal of Rock Mechanics and Mining Sciences, *48*(7), 1113–1122.

Battaglia, M. and Hill, D.P. (2009). *Analytical modeling of gravity changes and crustal deformation at volcanoes: The Long Valley caldera, California, case study*, Tectonophysics, *471* 45–57.

Battaglia M., Cervelli P.F. and Murray J.R. (2013), *Modeling crustal deformation near active faults and volcanic centers*—A catalog of deformation models: U.S. Geological Survey Techniques and Methods, book 13, chap. B1, 96 p., http://pubs.usgs.gov/tm/13/b1.

Barberi, G., Cocina, O., Maiolino, V., Musumeci, C. and Privitera, E. (2004). *Insight into Mt. Etna (Italy) kinematics during the 2002–2003 eruption as inferred from seismic stress and strain tensors*, Geophys. Res. Lett., *31*, L21614, doi:10.1029/2004GL020918.

Bonanno, A., Palano, M., Privitera, E., Gresta, S. and Puglisi, G. (2011). *Magma intrusion mechanisms and redistribution of seismogenic stress at Mt. Etna volcano (1997–1998)*, Terra Nova, *23*, 339–348, doi:10.1111/j.1365-3121.2011.01019.x.

Brandsdottir, B., and Einarsson, P. (1979). *Seismic activity associated with the September 1977 deflation of the Krafla central volcano in northern Iceland*, J. Volc. Geotherm. Res., *6*, 197–212.

Bruno, V., Mattia, M., Aloisi, M., Palano, M., Cannavò, F. and Holt, W.E.E. (2012). *Ground deformations and volcanic processes as imaged by CGPS data at Mt. Etna (Italy) between 2003 and 2008*, J. Geophys. Res., *117*, B07208, doi:10.1029/2011JB009114.

Cannavó, F. (2012). *Sensitivity analysis for volcanic source modeling quality assessment and model selection*, Computers & Geosciences, *44*, 52–59, doi:10.1016/j.cageo.2012.03.008.

Chiarabba, C., Amato, A., Boschi, E., and Barberi, F. (2000). *Recent seismicity and tomographic modeling of the Mount Etna plumbing system*, J. geophys. Res, *105* (B5), 10923–10938, doi:10.1029/1999JB900427.

Dieterich, J. (1994). *A constitutive law for rate of earthquake production and its application to earthquake clustering*, J. geophys. Res, *99*, 2601–2618.

Efron, B. (1982). *The Jackknife, bootstrap and other resampling plans*, Society for Industrial and Applied Mathematics, Philadelphia.

Herring, T.A., King, R.W. and McClusky, S.C. (2010). *Introduction to GAMIT/GLOBK, Release 10.4*, Department of Earth, Atmospheric and Planetary Sciences, Massachusetts Institute of Technology, Cambridge, MA.

McTigue, D.F. (1987). *Elastic stress and deformation near a finite spherical magma body: resolution of the point source paradox*, J. Geophys. Res., *92*(B12), 12931–12940, doi:10.1029/JB092iB12p12931.

Musumeci, C., Malone, S.D., Giampiccolo, E. and Gresta, S. (2000). *Stress tensor computations at Mount St. Helens (1995–1998),* Ann. Geofis., *43*(5), 889–904, doi:10.4401/ag-3681.

Nakamura, K., Jacob, K. H. and Davies, J. N. (1977). *Volcanoes as possible indicators of tectonic stress orientation: Aleutians and Alaska,* Pure Appl. Geophys., *115*, 87–112, doi:10.1007/BF01637099.

Palano, M., Puglisi, G. and Gresta, S. (2008). *Ground deformation patterns at Mt. Etna from 1993 to 2000 from joint use of InSAR and GPS techniques*, J. Volc. Geotherm. Res., *169* (3–4), 99–120, doi:10.1016/j.jvolgeores.2007.08.014.

Palano, M., Rossi, M., Cannavò, F., Bruno, V., Aloisi M., Pellegrino, D., Pulvirenti, M., Siligato, G. and Mattia, M. (2010). *Etn@ref: a geodetic reference frame for Mt. Etna GPS networks.* Ann. Geophys., *53*(4), 49–57, doi:10.4401/ag-4879.

Palano, M., Cannavò, F., Ferranti, L., Mattia, M. and Mazzella, M.E. (2011). *Strain and stress fields in the Southern Apennines (Italy) constrained by geodetic, seismological and borehole data,* Geophys. J. Int., *187*, 1270–1282, doi:10.1111/j.1365-246X.2011.05234.x.

Patanè, D., Privitera, E., Gresta, S., Akinci, A., Alparone, S., Barberi, G., Chiaraluce, L., Cocina, O., D'Amico, S., De Gori, P., Di Grazia, G., Falsaperla, S., Ferrari, F., Gambino, S., Giampiccolo, E., Langer, H., Maiolino, V., Moretti, M., Mostaccio, A., Musumeci, C., Piccinini, D., Reitano, D., Scarfì, L., Spampinato, S., Ursino, A., and Zuccarello, L. (2003). *Seismological constraints for the dike emplacement of July–August 2001 lateral eruption at Mt. Etna volcano, Italy*, Annals of geophysics, *46*(4), 599–608.

Pujol J. (2007). *The solution of nonlinear inverse problems and the Levenberg–Marquardt method*, Geophysics (SEG) *72* (4): W1–W16. doi:10.1190/1.2732552.

Reasenberg, P.A. and Oppenheimer, D. (1985). *FPFIT, FPPLOT and FPPAGE: fortran computer programs for calculating and displaying earthquake fault-plane solutions*, Open File Rep. *85–379*, 1–109, U. S. Geol. Surv., Washington.

Roman, D. C. (2005). *Numerical models of volcanotectonic earthquake triggering on non-ideally oriented faults*, Geophys. Res. Lett., *32*, L02304, doi:10.1029/2004GL021549.

Roman, D. C., Moran, S. C., Power, J. A. and Cashman, K. V. (2004). *Temporal and spatial variation of local stress fields during the 1992 eruptions of Crater Peak vent, Mount Spurr Volcano, Alaska,* Bull. Seismol. Soc. Am., *94*, 2366–2379, doi:10.1785/0120030259.

Rubin, A.M., Gillard, D., and Got, J.L. (1998). *A reinterpretation of seismicity associated with the January 1983 dike intrusion at Kilauea volcano, Hawaii*, J. geophys. Res, *103*, 10003–10015.

Segall, P. (2010). *Earthquake and volcano deformation*, Princeton, N.J., Princeton University Press, 458 p.

Segall, P. (2013). *Volcano deformation and eruption forecasting*, Geological Society, London, Special Publications, 380, doi:10.1144/SP380.4.

Tikhonov, A.N. and Arsenin, V.Y. (1977). *Solutions of Ill-Posed Problems*. New York: Winston. ISBN 0-470-99124-0.

Trasatti, E., Giunchi, C., and Bonafede, M. (2003). *Effects of topography and rheological layering on ground deformation in volcanic regions*, J. Volc. Geotherm. Res*., 122*, 89–110, doi:10.1016/S0377-0273(02)00473-0.

Umakoshi, K., Shimizu, H. and Matsuwo, N. (2001). *Volcano-tectonic seismicity at Unzen Volcano, Japan, 1985–1999,* J. Volc. Geotherm. Res, *112*, 117–131, doi:10.1016/S0377-0273(01)00238-4.

Williams, C. A., and Wadge, G. (2000). *An accurate and efficient method for including the effects of topography in three-dimensional elastic models of ground deformation with applications to radar interferometry*, J. geophys. Res, *105* (B4), 8103–8120, doi:10.1029/1999JB900307.

(Received February 11, 2013, revised November 15, 2013, accepted December 30, 2013)